# **Depth-Guided Camouflaged Object Detection**

Jing Zhang<sup>1</sup> Yunqiu Lv<sup>2</sup> Mochu Xiang<sup>2</sup> Aixuan Li<sup>2</sup> Yuchao Dai<sup>2</sup> \* Yiran Zhong<sup>1</sup>

Australian National University <sup>2</sup> Northwestern Polytechnical University zjnwpu@gmail.com, {lvyunqiu, xiangmochu, lax}@mail.nwpu.edu.cn, {daiyuchao, zhongyiran}@gmail.com

## **Abstract**

Camouflaged object detection (COD) aims to segment camouflaged objects hiding in the environment, which is challenging due to the similar appearance of camouflaged objects and their surroundings. Research in biology suggests that depth can provide useful object localization cues for camouflaged object discovery, as all the animals have 3D perception ability. However, the depth information has not been exploited for camouflaged object detection. To explore the contribution of depth for camouflage detection, we present a depth-guided camouflaged object detection network with pre-computed depth maps from existing monocular depth estimation methods. Due to the domain gap between the depth estimation dataset and our camouflaged object detection dataset, the generated depth may not be accurate enough to be directly used in our framework. We then introduce a depth quality assessment module to evaluate the quality of depth based on the model prediction from both RGB COD branch and RGB-D COD branch. During training, only high-quality depth is used to update the modal interaction module for multi-modal learning. During testing, our depth quality assessment module can effectively determine the contribution of depth and select the RGB branch or RGB-D branch for camouflage prediction. Extensive experiments on various camouflaged object detection datasets prove the effectiveness of our solution in exploring the depth information for camouflaged object detection. Our code and data is publicly available at: https: //github.com/JingZhang617/RGBD-COD.

## 1. Introduction

As a key example of evolution by natural selection, camouflage is widely adopted by the preys in wild to hide themselves in the surroundings and thus reduce their possibility of being detected or recognized by their predators [7]. Camouflaged Object Detection (COD) is the technology that

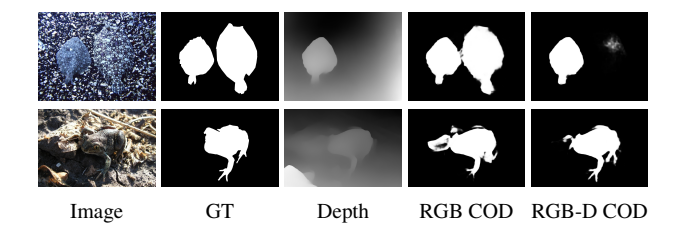


Figure 1. Our depth-guided camouflaged object detection network automatically determines the contribution of depth for camouflage detection, and performs RGB or RGB-D based camouflage detection during testing considering the estimated depth quality from the depth quality assessment module. The "RGB COD" and "RGB-D COD" are predictions from the RGB COD branch and RGB-D COD branch respectively.

segments the whole scope of the camouflaged object. It has wide applications in a variety of fields, such as military (*e.g.* military camouflaged pattern design [28]), agriculture (*e.g.* pest identification [39, 8]), medicine (*e.g.* polyp segmentation [15]) and ecological protection (*e.g.* wildlife protection [48, 72]. Due to both the scientific value and application value, COD deserves well exploration.

Compared with the generic object detection [59, 29] or segmentation techniques [4, 62], COD is more challenging as the foreground objects usually share a very similar appearance with their surroundings. The visual cues for object identification, *e.g.* texture, contrast, edge, color and object size, are vulnerable to attack from the basic camouflage strategies, *e.g.* background matching and disruptive coloration [67, 55]. Although some recent deep learning based studies [38, 76, 14, 11] have shown favorable performance, the misleading information in camouflage hinders the network from learning the discriminative features of camouflage. We argue that more visual perceptual knowledge about the camouflaged objects can be beneficial.

Inspired by research in biology, depth provides 3D geometric information that makes the observer more sensitive to the true boundary and thus enables camouflage less effective [1, 34]. Accordingly, combining depth with RGB image can serve as a new way to solve the challenges in

<sup>\*</sup>Corresponding author: Yuchao Dai (daiyuchao@gmail.com)

camouflaged object detection. Further, the visual system of many species operates in the real 3D scenes, and a lot of recent works for object segmentation [32, 17, 77, 56] have integrated depth map as another modal on top of RGB images to extract features about the 3D layout of the scene and object shape information.

As far as we know, there exists no deep camouflaged object detection model utilizing depth for effective camouflage detection. In this paper, we present the first depth-guided camouflaged object detection network to study the contribution of depth for camouflaged object detection. As there is no RGB-D camouflaged object detection dataset, we generate depth map of the COD training dataset [14] with existing monocular depth estimation method [58].

With the estimated depth, a straightforward way to achieve RGB-D COD is through different fusion strategies following the multi-modal learning pipelines. However, the conventional monocular depth estimation models are trained on natural images, where there may not exist any camouflaged objects. The domain gap of the monocular depth estimation training dataset and COD training dataset leads to less accurate (or noisy) depth maps. Directly training with the noisy depth map may lead to an over-fitting model that generalizes poorly on the testing dataset.

To study the contribution of depth for camouflage detection, we need to assess the depth quality and avoid the noisy depth map from contributing too much in model learning. With this goal, we introduce a depth quality assessment module to estimate the quality of depth. Specifically, we first generate depth map for our COD training dataset using the monocular depth estimation method. Then, we design an RGB COD network and RGB-D COD network as shown in Fig. 2 with some parts of the network sharing weights. Within the RGB-D COD network, we introduce an auxiliary depth estimation module to set constraints on the depth features. Further, to eliminate the domain gap in our depth data, we present a depth quality assessment module for depth quality estimation with predictions from RGB COD and RGB-D COD branches as guidance. During training, the modal interaction part is updated only with highquality depth. During testing, the depth estimation module is used to estimate depth quality and decide which branch (RGB COD or RGB-D COD) to be used for camouflaged object detection. In Fig. 1, we show predictions of our network. The depth map in the first row has one missed camouflaged instance, leading to inferior prediction than the RGB COD network. The depth map in the second row is accurate enough to train an effective RGB-D COD network, leading to better performance.

Our main contributions are summarized as: 1) We advocate the contribution of depth for camouflaged object detection, and propose the first depth-guided camouflaged object detection network; 2) We introduce depth quality assessment module to evaluate the quality of depth for camouflage detection, and only update the modal interaction part of the network ("Mode Exploring" in Fig. 2) with the high-quality depth; 3) During testing, our depth quality assessment module can automatically identify the quality of depth to perform RGB COD or RGB-D COD accordingly.

# 2. Related Work

Camouflaged Object Detection Camouflage is a defense mechanism for animals to change their salient signatures and become invisible in the environment [7]. In early time, many researchers have developed extensive methods using hand-crafted features such as edge, brightness, color, gradient, texture to detect the camouflaged object [66, 2, 22, 75, 54, 41]. However, these algorithms are far from the practical application because the well-performed camouflage is skilled in breaking the low-level features. Research in COD [81, 18, 38, 76, 14, 11] turn to deep neural network in order to borrow its powerful representative ability to extract high-level semantic features to discriminate the concealed object from the complex scenarios. Although recent methods based on deep learning have made great progress in performance, they only encode RGB images, which provide limited information about the 3D structure. [34] claims that cuttlefish makes use of low-level cues to disrupt the perception of visual depth and therefore disguise their 3D shape. As described in [51], seeing the environment in 3D makes the presence of the object easier to be discerned. [1] verifies that the real 3D structure information provided by the depth is advantageous to overcome the disruption caused by edge enhancement. Therefore, in this paper, we resort to the depth map as additional cues for the detection, and experimentally prove the effectiveness of depth for camouflaged object detection.

**Depth-Guided Object Detection** For segmentation task, many studies have been shown that the depth information can reduce the ambiguity of RGB features in complex scenarios. In early works of semantic segmentation [64, 61, 27, 9] and salient object segmentation [52, 60, 20, 69], depth map and RGB image are respectively represented by handcrafted features and models are constructed based on the features. In recent years, benefiting from the powerful deep learning, many studies demonstrate that deep cross-modal fusion for segmentation has achieved performance improvement. [19] proposes a simple early fusion to concatenate the RGB and depth channels and feed the input into a multiscale CNN network. [46] fuses the maps from the depth, RGB and early fusion branch at decision level, which is called late fusion. To obtain more accurate and robust segmentation, a variety of models delicately design strategies to merge the complementary information in the middle level of the network [50, 68, 43, 20, 45, 3, 53]. For camouflaged object detection, the main concern lies in solutions to fuse

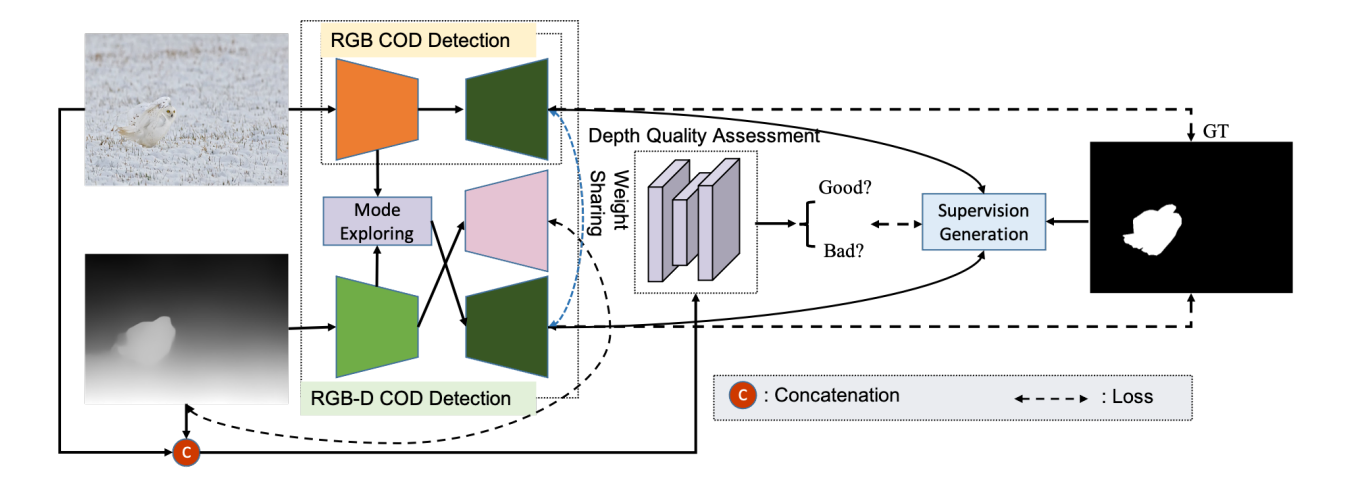


Figure 2. Three main modules are included in our framework: 1) a "RGB COD" module to perform RGB image COD; 2) a "RGB-D COD" module with auxiliary depth estimation module for RGB-D COD and depth estimation. 3) a "Depth Quality Assessment" module to estimate depth quality based on the accuracy of predictions from the "RGB COD" branch and "RGB-D COD" branch. During training, the estimated quality from the "Depth Quality Assessment" determines whether the "Mode Exploring" should be updated. During testing, we estimate the quality of test images to automatically determine the branch (RGB COD or RGB-D COD) for camouflaged object detection.

the high-quality depth with the RGB image.

Confidence-aware Learning Our depth quality assessment module is designed to evaluate the depth quality, which is a confidence-aware learning strategy to effectively identify quality of the depth. Confidence-aware learning aims to produce the confidence maps representing the awareness of prediction (epistemic uncertainty) or the quality of the data (aleatoric uncertainty) [35]. In this paper, as we mainly focus on modeling the quality of depth, we only discuss the aleatoric uncertainty modeling strategies. [36] designs a network which yields a probabilistic distribution as output in order to capture such uncertainty. [63] employs a teacher-student paradigm to distill the aleatoric uncertainty. The teacher network generates multiple predicative samples by incorporating aleatoric uncertainty for the student network to learn. [37] uses adversarial perturbation technique to generate additional training data for the model to capture the aleatoric uncertainty.

Uniqueness of our solution Different from the existing camouflaged object detection methods [38, 76, 14, 47] which rely only on the RGB images, we introduce the first depth-guided camouflaged object detection framework, with a depth quality assessment module to automatically identify the quality of the depth. Our depth quality assessment module directly produces a scalar in the range of [0, 1] representing depth quality. Although there exist ensembles [10, 37] or dropout techniques [24] that can be used in our scenario for depth quality assessment, they usually involve multiple copies of the network (ensembles based) or multiple iterations of inference (dropout based). Our depth quality assessment network directly output depth quality measure, which is more efficient to implement.

# 3. Our Method

We introduce a depth-guided camouflaged object detection network to study the contribution of depth for camouflaged object detection, and show the pipeline of our framework in Fig. 2. To start our pipeline, we first generate the depth map with existing monocular depth estimation methods, and then we introduce the depth quality assessment module to effectively identify the high-quality depth based on the model prediction from the RGB COD and RGB-D COD, and update network parameters accordingly.

# 3.1. Initial Depth Generation

As there exists no RGB-D based camouflaged object detection dataset, we generate pseudo depth maps from existing monocular depth estimation methods. We used three state-of-the-art monocular depth estimation methods (MiDaS[58], Monodepth2[26] and FrozenPeople[42]) to generate depth maps for our training and testing dataset.

Trained on 10 different RGB-D datasets, MiDaS [58] provides robust results across diverse scenes. Targeting autonomous driving, Monodepth2 [26] has a good performance on the KITTI benchmark under the self-supervision, but its ability of domain adaption is to be investigated. Since there are a large number of images with humans as camouflaged objects in our camouflage training dataset, we use FrozenPeople [42] with the single image configuration to generate depth for the characters in the scene.

Both MiDaS and Monodepth2 generate depth map in the form of disparity, or inverse-depth, FrozenPeople generates depth values directly. We show the generated depth maps for our camouflaged object detection dataset in Fig. 3. Due

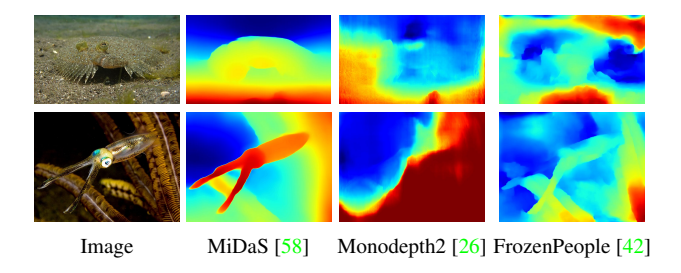


Figure 3. Camouflage images and the generated depth maps. Three methods are used to generate depth maps. Overall, MiDaS [58] has the best cross dataset performance and the strongest generalization ability. MonoDepth2 [26] is trained only on KITTI dataset, which performs the worst in our scenario.

to the visually better performance of MiDaS depth maps<sup>1</sup>, we adopt MiDaS depth maps in our experiments.

#### 3.2. Depth Quality Assessment

Due to the domain gap, the generated depth map from monocular depth estimation methods may not be very accurate as shown in Fig. 3. Directly training with the less-accurate depth map may not improve the model performance as the network will over-fit on the less-accurate depth map, leading to poor generalization ability (We explained this phenomenon in the experiments section). Instead of directly using the depth, we aim to estimate its quality first, and then use only the high-quality depth for multi-modal (RGB mode and depth mode) information exploring.

Our RGB camouflaged object detection training dataset is given as  $D = \{x_i, y_i\}_{i=1}^N$ , where  $x_i$  and  $y_i$  are the RGB image and corresponding camouflage map. i indexes the training dataset of size N. We define the generated depth map from the monocular estimation method, e.g. Mi-DaS [58] depth in particular, as  $d_i$ . Our goal is to estimate quality of  $d_i$  given  $x_i$  and  $y_i$  for effective depth-guided camouflaged object detection as shown in Fig. 2. Three main modules are included in our framework, namely a "RGB COD" module, a "RGB-D COD" module and a "Depth Quality Assessment" module.

#### 3.2.1 RGB COD model

The RGB COD network is built upon ResNet50 [30] as shown in Fig. 4. There exist four stages of features in the backbone network, denoting as  $\{s_k\}_{k=1}^4$ . The RGB COD network is composed of an "Encoder" and a "Decoder". The former is our backbone network with four stages of features. The latter aims to integrate higher-lower features with a larger receptive field for camouflage object detection. Specifically, we feed  $\{s_k\}_{k=2}^4$  to the atrous spatial pyramid pooling module (ASPP) [4] with different rates of atrous

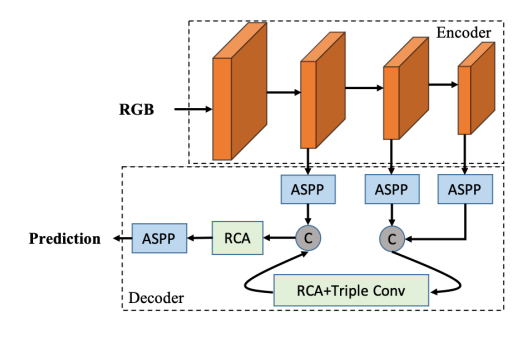


Figure 4. The RGB COD network, where "ASPP" is the atrous spatial pyramid pooling module [4], and "RCA" is the residual channel attention module [79].

convolution for various scales of context information modeling, and we then obtain  $\{s'_k\}_{k=2}^4$  of channel size C=32.

We concatenate  $s_4'$  with  $s_3'$  and feed it to a residual channel attention [79] ("RCA" module) to extract discriminative feature  $s_{43}'$  of channel size 2\*C. Then, we feed  $s_{43}'$  to three cascaded  $3\times 3$  convolutional layer ("Triple Conv") of channel size C and concatenate it with  $s_2'$ . Similarly, we attach one residual channel attention for discriminative feature generation. The feature after the attention module is fed to the last ASPP module to produce our camouflage prediction for the RGB COD branch. Let's define the parameter set of the RGB COD network as  $\theta = \{\theta_e, \theta_d\}$ , representing parameter set for the "Encoder" and "Decoder" respectively. The prediction of the RGB COD module is then defined as  $f_{\theta}(x)$ . We omit i for simplicity.

#### 3.2.2 RGB-D COD model

The RGB-D COD model  $g_{\beta}$  ( $\beta$  is network parameter set) takes both RGB image and depth data as input, and produces camouflage map  $g_{\beta}^c$  with an auxiliary depth estimation module to regress the depth map  $g_{\beta}^d$  as shown in Fig. 5. We introduce the auxiliary depth estimation module to prevent network over-fitting on the low-quality depth data.

**Mode Exploring:** The RGB encoder is the same as the encoder in the RGB COD module. Similar to RGB encoder, the depth encoder is also built upon ResNet50 [30]. We have backbone feature for the RGB encoder as  $\{s_k\}_{k=1}^4$ . We then define backbone feature for the depth encoder as  $\{s_k\}_{k=1}^4$ . The "Mode Exploring" module aims to effectively fuse the RGB feature and depth feature for multimode learning. Specifically, we add one  $3\times 3$  convolutional layer after each of  $s_k$  and  $s_k^d$ , to obtain the channel-reduced RGB feature and depth feature of channel size C=32. Then, for the feature of each stage, we concatenate the RGB feature with the depth feature, and feed it to RCA [79] for discriminative feature extraction. Finally, we add another  $3\times 3$  on top of RCA to obtain fuse multi-stage feature  $\{s_k^f\}_{k=1}^4$  of same channel size as  $\{s_k\}_{k=1}^4$  accordingly.

<sup>&</sup>lt;sup>1</sup>The "depth map" represents "inverse-depth map" in the following.

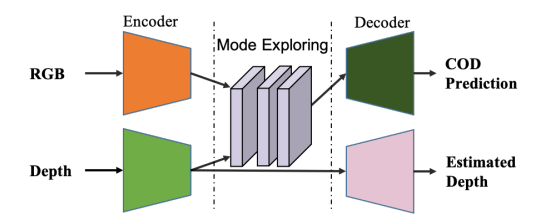


Figure 5. The RGB-D COD network, where structures of RGB "Encoder" and "Decoder" are same as in Fig. 4.

**The Decoder:** Two sets of decoders are included in our RGB-D COD module, namely a COD prediction decoder and a depth estimation decoder. We define the COD prediction decoder same as "Decoder" in Fig. 4, and they also share weights. Only that the COD prediction module takes  $\{s_k^f\}_{k=1}^4$  after the "Mode Exploring" as input. For the depth estimation module, we design a U-Net shape module. Given the depth feature  $\{s_k^d\}_{k=1}^4$  from the depth encoder, we gradually integrate higher level feature with lower level feature. Specifically, for higher level feature  $s_k^d$  and lower level feature  $s_{k-1}^d$ , the integrated feature is defined as:

$$s_{k-1,k} = Cat(Up2(ELU(Conv3 \times 3(s_k^d))), s_{k-1}^d),$$
 (1)

where  $Conv3 \times 3$  is a  $3 \times 3$  convolutional layer of channel size same as  $s_{k-1}^d$ , ELU is the ELU activation function, Up2 is 2 times bilinear upsampling, Cat is the concatenation operation. After gradually high-low feature integration, we add one  $3 \times 3$  convolutional layer in the end to generate a one channel depth map d'.

**Parameters:** As shown in Fig. 2 and Fig. 5, the RGB COD decoder shares weights with the RGB-D COD decoder. COD prediction in Fig. 5 is controlled by RGB encoder, depth encoder, "Mode Exploring", and COD decoder. The estimated depth is achieved via the depth encoder and depth decoder. We argue that both high and low-quality depth map can be used to update the depth encoder and depth decoder, as the smoothness loss [70] in the depth assessment module can push the network to generate relatively effective depth feature (we introduce the loss function in section 3.2.4). However, the "Mode Exploring" module is very sensitive to the depth quality. We then update it only with the high-quality depth maps.

# 3.2.3 Depth Quality Assessment

As discussed above, due to the domain gap, the generated depth map may not be very accurate. Training directly with less accurate depth data as input may decrease model generalization ability. Further, we argue that although there exist low-quality depth maps, we can still observe a large amount of reasonable depth maps. Instead of using all the depth data to update our whole framework, we intend to select the

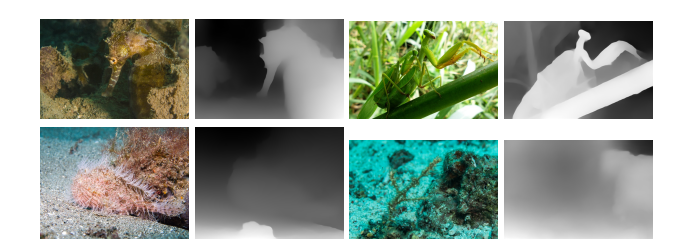


Figure 6. The selected high-quality depth (first row) and low-quality depth (second row).

high-quality depth maps to contribute more to our camouflaged object detection task.

Network Structure: The depth quality assessment module is composed of four cascaded convolutional layers of kernel size 3 and stride size 2 and one fully connected layer to produce a scalar in the range of [0,1] representing depth quality. The RGB image and depth map are concatenated and feed to the depth quality assessment network. The the channel size of the four convolutional layers are C, 2\*C, 4\*C, C respectively. Batch normalization and LeakyReLU are used after all the convolutional layers. The last fully connected layer is used to map the feature map of channel size C to a two-dimensional feature vector representing depth quality. We define depth assessment module as  $q_{\gamma}$ , where  $\gamma$  is the parameter set.

**Supervision Generation:** As shown in Fig. 2, the depth quality assessment module is designed to estimate the quality of depth. As we have no prior knowledge about the depth quality, we introduce a performance-guided depth quality supervision generation technique. Specifically, we compute camouflage map from the RGB branch as  $f_{\theta}(x)$ . We also obtain the camouflage map from the RGB-D branch as  $g_{\beta}^{c}(x,d)$ . Our assumption is that, with the same RGB image, the higher accuracy of  $g_{\beta}^{c}(x,d)$  compared with  $f_{\theta}(x)$  indicates positive contribution or higher quality depth map. We then define the supervision for the depth assessment module as  $c = \{1,0\}$  ("Good"). Otherwise, we define its corresponding supervision as  $c = \{0,1\}$  ("Bad"). In Fig. 6, we show the selected high/low-quality depth with our performance-guided supervision<sup>2</sup>.

## 3.2.4 Objective Function

As shown in Fig. 2, we have COD prediction from the RGB COD branch  $f_{\theta}(x)$  and COD prediction from the RGB-D COD branch  $g^c_{\beta}(x,d)$ . Furthermore, we have a depth estimation module  $g^d_{\beta}(x,d)$  to estimate the depth, thus reduces the negative effects from the lower quality depth maps. We

 $<sup>^2{\</sup>rm The}$  output from the depth quality assessment module is normalized with the Sigmoid function and binarized with 0.5 to obtain depth quality measure in  $\{0,1\}$ 

also have a depth quality assessment module  $q_{\gamma}(x,d)$  to estimate pixel-wise depth quality. In this way, our final loss function includes four parts as:

$$\mathcal{L} = \mathcal{L}_{ce}(f_{\theta}(x), y) + \mathcal{L}_{ce}(g_{\beta}^{c}(x, d), y) + \mathcal{L}_{ce}(q_{\gamma}(x, d), c) + \mathcal{L}_{d},$$
(2)

where  $\mathcal{L}_{ce}$  is the binary cross-entropy loss,  $\mathcal{L}_d$  is the depth estimation loss. In this paper, we define it as weighted sum of smooth L1 loss and smoothness loss [70]. The smooth L1 loss  $(L_1(g^d_\beta(x,d),d)))$  measures the accuracy of predicted depth map  $d'=g^d_\beta(x,d)$  compared with the generated depth map d from [58]. The smoothness loss constrains the depth to share similar structure as our ground truth camouflage map, which is defined as:

$$\mathcal{L}_s = \sum_{u,v} \sum_{d \in \overrightarrow{x}, \overrightarrow{y}} \Psi(|\partial_d d'_{u,v}| e^{-\alpha |\partial_d y(u,v)|}), \qquad (3)$$

where  $\Psi$  is defined as  $\Psi(s) = \sqrt{s^2 + 1e^{-6}}$ ,  $d'_{u,v}$  is the predicted depth map at position (u,v), d indexes over partial derivative in  $\overrightarrow{x}$  and  $\overrightarrow{y}$  directions. We set  $\alpha=10$  in our experiments following the setting in [70]. In this way, our depth estimation loss is defined as:

$$\mathcal{L}_d = \lambda_1 L_1(g_\beta^d(x, d), d) + \lambda_2 \mathcal{L}_s, \tag{4}$$

where  $\lambda_1$  and  $\lambda_2$  are used to control the contribution of each loss for the depth estimation loss as well as the contribution of depth loss for our final loss function in Eq. 2. Empirically, we set  $\lambda_1=10$  and  $\lambda_2=0.5$  to achieve similar range of  $\lambda_1 L_1$  and  $\lambda_2 L_s$ . We experimented with different setting of  $\lambda_1$  and  $\lambda_2$ , and found robust performance if the two loss terms are balanced.

# Algorithm 1 Depth-Guided Camouflage Detection

#### Input:

- (1) Training dataset  $D = \{x_i, d_i, y_i\}_{i=1}^N$ , where the depth map  $d_i$  is pre-computed from [58].
- (2) The maximal number of learning epochs E.

**Output**: Model parameter  $\theta$  for the RGB COD branch,  $\beta$  for the RGB-D COD branch, and  $\gamma$  for the depth estimation module;

- 1: **for**  $t \leftarrow 1$  to E **do**
- 2: Generate camouflage map  $f_{\theta}(x_i)$  from the RGB COD branch, and  $g_{\beta}(x_i, d_i)$  from the RGB-D COD branch for  $x_i$ .
- 3: Compute accuracy  $a_{\theta}$  of  $f_{\theta}(x_i)$  and  $a_{\beta}$  of  $g_{\beta}(x_i, d_i)$  based on ground truth  $y_i$ ;
- 4: if a<sub>θ</sub> < a<sub>β</sub>, d<sub>i</sub> belong to the high-quality depths, and we define its supervision c<sub>i</sub> for the depth estimation module as 1. Otherwise, c<sub>i</sub> = 0, indicating low quality depth map;
- 5: Feed concatenation of  $x_i$  and  $d_i$  to the depth estimation model and obtain  $e_{\gamma}(x_i, d_i)$ ;
- 6: Update parameter  $\gamma$  of the depth estimation module with  $\mathcal{L}_{ce}(e_{\gamma}(x_i,d_i),c_i);$
- 7: If  $c_i=1$ , update parameter  $\beta$  the RGB-D COD branch. Otherwise, only update parameter  $\theta$  of the RGB COD branch.
- 8: end for

**Training solution:** As discussed above, only high-quality depth is used to update the "Mode Exploring" module. For the image with high-quality depth, it will be used to train our entire framework. For the image with low-quality depth, the RGB encoder, COD decoder in the RGB-D COD module are updated with only the RGB image. The depth is only used to update the depth estimation module. We show the whole learning pipeline of our method in Algorithm 1.

# 4. Experimental Results

# **4.1. Setup**

**Datasets** We train our method with COD10K [14] training dataset, which contains 4,040 images with corresponding ground truth camouflage maps following SINet [14]. We then test model performance on four benchmark camouflage testing datasets, including CAMO [38] of size 250, CHAMELEON of size 76, COD10K testing sets of size 2,026, and the newly released NC4K dataset [47] of size 4.121.

**Evaluation Metrics** Four widely used metrics are employed for performance evaluation, including 1) Mean Absolute Error  $(\mathcal{M})$ ; 2) Mean F-measure  $(F_{\beta})$ ; 3) Mean E-measure  $(E_{\xi})$  [13]; 4) S-measure  $(S_{\alpha})$  [12]. Details of those evaluation metrics are introduced in the supplementary materials.

Compared Methods Since there exists limited work on camouflaged object detection [14, 47, 76, 38], similar to [47], considering the similarity of saliency detection and camouflage detection, we re-train saliency detection models with COD10K training dataset, and provide benchmark performance in Table 1, where we do not re-train SINet [14] and LSR [47], and only test their predictions with the provided models.

Implementation Details We train our model in Pytorch with ResNet-50 as backbone for the encoders, which is initialized with weights trained on ImageNet, and other newly added layers are randomly initialized. We resize all the images and ground truth to  $352\!\times\!352$  for both training and testing. The maximum epoch is 50. The initial learning rates are  $5\times10^{-5}$  and  $2.5\times10^{-5}$  for the camouflaged object detection network (both RGB branch and RGB-D branch) and depth quality assessment network respectively. The whole training takes 17 hours with batch size 6 on one NVIDIA GTX 2080Ti GPUs.

# 4.2. Performance comparison

Quantitative comparison: We compare our results with the benchmark models we generated in Table 1, where SINet [14] and LSR [47] are two RGB image based camouflaged object detection methods. Our final results ("Ours") show consistent better performance compared with the benchmark models. Further, as a RGB-D camouflaged

TE 1 1 1 D C	• • • • • • • • • • • • • • • • • • • •	1 1 1	a 11.	. 1	1 1 1 1 1 1 1 1 1 1 1 1 1 1 1 1 1 1 1 1
Table I Performance com	naricon with	henchmark camou	flaged object	t detection models on	benchmark testing datasets.
Table 1. I childinance com	parison with	ochemiark camou	mageu object	detection models on	belieffillark testing datasets.

Table I	i. Perio	CAMO [38]					ELEON [65]	ged obj	ect dete	COD10		on bene	NC4K [47]				
Method	$S_{\alpha} \uparrow$	$F_{\beta} \uparrow$	$E_{\xi} \uparrow$	$\mathcal{M}\downarrow$	$S_{\alpha} \uparrow$	$F_{\beta} \uparrow$	$E_{\xi}^{\mathrm{mean}} \uparrow$	$\mathcal{M}\downarrow$	$S_{\alpha} \uparrow$	$F_{\beta} \uparrow$	$E_{\xi} \uparrow$	$\mathcal{M}\downarrow$	$S_{\alpha} \uparrow$	$F_{\beta} \uparrow$	$E_{\xi} \uparrow$	$\mathcal{M}\downarrow$	
Wictiou	υα	1 β	Lξ	<i>7</i> 01 \$	Θα Ι	1. B		B COD	_	1. B	£ξ	JV1 4	υα Ι	I B	Εξ	<i>7</i> <b>1</b> ↓	
CPD [73]	0.716	0.618	0.723	0.113	0.857	0.771	0.874	0.048	0.750	0.595	0.776	0.053	0.790	0.708	0.810	0.071	
SCRN [74]	0.779	0.705	0.725	0.090	0.876	0.787	0.889	0.042	0.789	0.651	0.817	0.033	0.832	0.759	0.855	0.059	
CSNet[25]	0.771	0.705	0.795	0.092	0.856	0.766	0.869	0.047	0.778	0.635	0.810	0.047	0.819	0.748	0.845	0.061	
PoolNet [44]	0.730	0.643	0.746	0.105	0.845	0.749	0.864	0.054	0.740	0.576	0.776	0.056	0.785	0.699	0.814	0.073	
F3Net [71]	0.711	0.616	0.741	0.109	0.848	0.770	0.894	0.047	0.739	0.593	0.795	0.051	0.782	0.706	0.825	0.069	
ITSD[82]	0.750	0.663	0.779	0.102	0.814	0.705	0.844	0.057	0.767	0.615	0.808	0.051	0.811	0.729	0.845	0.064	
BASNet [57]	0.615	0.503	0.671	0.124	0.847	0.795	0.883	0.044	0.661	0.486	0.729	0.071	0.698	0.613	0.761	0.094	
EGNet [80]	0.737	0.655	0.758	0.102	0.856	0.766	0.883	0.049	0.751	0.595	0.793	0.053	0.796	0.718	0.830	0.067	
R2Net [21]	0.772	0.685	0.777	0.098	0.861	0.766	0.869	0.047	0.787	0.636	0.801	0.048	0.823	0.739	0.835	0.064	
RASNet [5]	0.763	0.716	0.824	0.090	0.857	0.804	0.923	0.040	0.778	0.673	0.865	0.044	0.817	0.772	0.873	0.057	
SINet [14]	0.745	0.702	0.804	0.092	0.872	0.827	0.936	0.034	0.776 0.67	0.679	0.864 0.868	0.043	0.810	0.772		0.057	
LSR [47]	0.793	0.725	0.826	0.085	0.893	0.839	0.938	0.033	0.793	0.793 0.685		0.041	0.839	0.779	0.883	0.053	
							RGI	B-D COI	Models								
UCNet [77]	0.729	0.672	0.785	0.101	0.869	0.823	0.924	0.039	0.738	0.611	0.825	0.052	0.784	0.728	0.849	0.066	
BBSNet [17]	0.776	0.689	0.786	0.093	0.864	0.768	0.872	0.049	0.782	0.633	0.836	0.050	0.825	0.745	0.859	0.062	
JL-DCF [23]	0.772	0.670	0.777	0.102	0.857	0.734	0.867	0.052	0.749	0.581	0.789	0.053	0.788	0.713	0.819	0.072	
SSF [78]	0.748	0.643	0.782	0.116	0.866	0.788	0.904	0.045	0.729	0.593	0.778	0.055	0.770	0.689	0.827	0.069	
Ours	0.801	0.773	0.852	0.076	0.898	0.856	0.954	0.029	0.809	0.711	0.881	0.037	0.842	0.801	0.897	0.047	
		**			7	7	6	4	*	:	*	ı	ď		A	K	
		\ \ \ \ \ \ \ \ \ \ \ \ \ \ \ \ \ \ \	2	ear	7-3	9		Q.	<b>y</b> -	, 5					4	<b>,</b>	
						4					7.						

Figure 7. Visual comparison of our predictions with the benchmark techniques.

CSNet [25]

EGNet [80]

object detection network, we also re-train four RGB-D saliency detection networks (UCNet [77], BBSNet [17], JL-DCF [23], SSF [78]) with the RGB-D camouflaged object detection dataset with depth maps generated by [58]. We notice a big performance gap between the best RGB-D model (BBSNet [17] in particular) and the state-of-the-art RGB model (LSR [47]). The main reason is the low quality depth data may lead to model of poor generalization ability. With the proposed depth quality assessment model, we can automatically decide the appropriate branch (RGB COD or RGB-D COD) for camouflaged object detection.

GT

ITSD [82]

Image

**Qualitative comparison:** In Fig. 7, we show four samples with predictions from benchmark techniques and our solution. Depth maps in the first and last rows are inferior to provide useful information for camouflaged object detec-

tion, and our depth quality assessment module can then define it as "bad" depth, and the RGB COD network is called for camouflaged object detection. For depth maps in the second and third row, their qualities are "good" according to the depth quality assessment module, and our better prediction compared with benchmark solutions illustrates the effectiveness of our method.

Depth

Ours

SINet [14]

Running time comparison: Although dual-branch, the parameter number of our model is 73M, which is comparable with UCNet [77] (62M), BBSNet [17] (49M), and much smaller than JL-DCF [23] (144M). During inference, our depth quality assessment module is used to estimate depth quality and decide RGB COD or RGB-D COD to be used. In this way, only one COD branch is used during inference, which leads to a mean inference time of 0.02s/image, and it

Table 2.	Performance	of ablation	study	models.

		CAM	O [38]			CHAMI	ELEON [65]			COD10	K [14]		NC4K [47]					
Method	$S_{\alpha} \uparrow$	$F_{eta}\uparrow$	$E_{\xi} \uparrow$	$\mathcal{M}\downarrow$	$S_{\alpha} \uparrow$	$F_{eta}\uparrow$	$E_{\xi}^{\mathrm{mean}} \uparrow$	$\mathcal{M}\downarrow$	$S_{\alpha} \uparrow$	$F_{\beta}\uparrow$	$E_{\xi} \uparrow$	$\mathcal{M}\downarrow$	$S_{\alpha} \uparrow$	$F_{\beta}\uparrow$	$E_{\xi} \uparrow$	$\mathcal{M}\downarrow$		
Ours	0.801	0.773	0.852	0.076	0.898	0.856	0.954	0.029	0.809	0.711	0.881	0.037	0.842	0.801	0.897	0.047		
M1	0.790	0.748	0.844	0.079	0.882	0.826	0.936	0.033	0.794	0.688	0.867	0.041	0.836	0.790	0.892	0.050		
M2	0.782	0.746	0.839	0.081	0.886	0.830	0.944	0.030	0.781	0.667	0.856	0.042	0.824	0.775	0.882	0.053		
M3	0.783	0.730	0.832	0.085	0.885	0.831	0.936	0.031	0.797	0.690	0.866	0.041	0.836	0.789	0.890	0.051		
M4	0.780	0.733	0.824	0.086	0.886	0.837	0.939	0.031	0.792	0.692	0.856	0.040	0.828	0.784	0.876	0.053		
M5	0.794	0.756	0.846	0.078	0.891	0.849	0.943	0.031	0.801	0.706	0.872	0.038	0.838	0.797	0.894	0.049		

is comparable with benchmark techniques.

# 4.3. Ablation Study

We propose a depth-guided camouflaged object detection network, with a depth quality assessment module to evaluate depth quality and only select high-quality depth for depth related layers updating. We analyze our model in this section, and show the performance in Table 2.

**Training directly the RGB COD network:** We train directly our RGB COD network as shown in Fig.4, and report its performance as "M1". We notice the similar performance of "M1" compared with benchmark methods in Table 1, which indicates effectiveness of the proposed RGB COD baseline module.

Training directly the RGB-D detection network: With depth from monocular depth estimation method, we can train directly the RGB-D COD task. As a multi-modal learning pipeline, we introduce three different settings, namely early fusion model ("M2"), cross-level fusion model ("M3") and late fusion model ("M4"). For "M2", we concatenate x and d in the input layer, and feed it to a  $3 \times 3$  convolutional layers to obtain a feature map of channel size 3. Then we feed the 3 channel feature map to the RGB COD network to produce camouflage prediction. For "M3", we remove the depth estimation decoder from Fig. 5. For "M4", we have two copies of RGB COD network that take RGB or depth as input to produce two copies of predictions. We concatenate the two predictions and feed it to a 3 × 3 convolutional layers to produce our final prediction. Deeply supervision is applied to each of the COD networks. With the depth maps from monocular depth estimation method, we observe the similar performance of the three fusion strategies, which is in general inferior to "M1". One conclusion we can draw from these experiments is that directly using the less accurate depth map may not be beneficial for effective multi-modal learning.

**Training the RGB-D detection network with auxiliary depth estimation module:** We argue that training directly with the less accurate depth map may lead to a model of poor generalization ability. We then introduce an auxiliary depth estimation module as shown in Fig. 5 to decrease the negative effect of low-quality depth. We train directly the RGB-D COD network in Fig. 5, and show it's performance as "M5". In this way, "M5" is "M3" with auxiliary depth

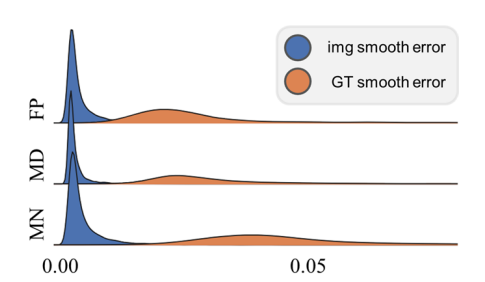


Figure 8. Smoothness error of depth generated with different monocular depth estimation techniques.

estimation module. We observe the consistent better performance of "M5" compared with both "M3" and "M1", which explains two conclusions: 1) the auxiliary depth estimation module can improve model performance with the depth of low quality; 2) the depth data can indeed provide useful geometric information for effective multi-modal learning.

#### 4.4. Analysis

Depth contribution: In general, we observe improved performance of "M1" compared with "M2". We then compute MAE of each sample, and find that "M2" performs better on some samples, while it performs worse on samples where the depth fails to distinguish the camouflaged objects and the background. Further, we compare "M2", "M3" and "M4", and find three observations: 1) if the depth of the camouflaged objects is obvious, the early fusion model ("M2") usually achieves better performance; 2) if the depth of the camouflaged objects can not be easily distinguished, the late fusion model ("M4") can prevent the network from generating false-positive regions; 3) the cross-level fusion model usually achieves the best performance within the three fusion strategies.

**Depth generation models:** We compute the smoothness error [70] of each depth data with image and ground truth camouflage map as references respectively, and show the results in Fig. 8. The relative consistent smoothness error with regard to image is due to the insufficient structure information in the camouflaged images. The smaller smoothness error of MD (MiDaS [58]) compared with MN (Monodepth2 [26]) indicates better depth maps from MiDaS depth estimation network. Trained on the most extensive data set, the depth map generated by MiDaS [58] already contains a

Table 3. Performance comparison of the depth from different monocular depth estimation solutions.

		CAMO	O [38]			CHAMI	ELEON [65]			COD10	K [14]		NC4K [47]				
Method	$S_{\alpha} \uparrow$	$F_{\beta} \uparrow$	$E_{\xi} \uparrow$	$\mathcal{M}\downarrow$	$S_{\alpha} \uparrow$	$F_{\beta} \uparrow$	$E_{\xi}^{\mathrm{mean}} \uparrow$	$\mathcal{M}\downarrow$	$S_{\alpha} \uparrow$	$S_{\alpha} \uparrow F_{\beta} \uparrow$		$\mathcal{M}\downarrow$	$S_{\alpha} \uparrow$	$F_{\beta} \uparrow$	$E_{\xi} \uparrow$	$\mathcal{M}\downarrow$	
LSR [47]	0.793	0.725	0.826	0.085	0.893	0.839	0.938	0.033	0.793	0.685	0.868	0.041	0.839	0.779	0.883	0.053	
Ours	0.801	0.773	0.852	0.076	0.898	0.856	0.954	0.029	0.809	0.711	0.881	0.037	0.842	0.801	0.897	0.047	
M1	0.790	0.748	0.844	0.079	0.882	0.826	0.936	0.033	0.794	0.688	0.867	0.041	0.836	0.790	0.892	0.050	
FP	0.798	0.756	0.856	0.078	0.888	0.835	0.939	0.032	0.801	0.701	0.877	0.038	0.839	0.795	0.893	0.049	
MN	0.796	0.754	0.850	0.079	0.885	0.835	0.935	0.032	0.803	0.706	0.875	0.037	0.838	0.798	0.891	0.048	

Table 4. Performance comparison of the depth mixup solution and ours.

		CAM	O [38]			CHAMI	ELEON [65]			COD10	K [14]		NC4K [47]				
Method	$S_{\alpha} \uparrow$	$F_{\beta} \uparrow$	$E_{\xi} \uparrow$	$\mathcal{M}\downarrow$	$S_{\alpha} \uparrow$	$F_{\beta} \uparrow$	$F_{\beta} \uparrow E_{\xi}^{\mathrm{mean}} \uparrow$		$S_{\alpha} \uparrow$	$S_{\alpha} \uparrow F_{\beta} \uparrow$		$\mathcal{M}\downarrow$	$S_{\alpha} \uparrow$	$F_{\beta} \uparrow$	$E_{\xi} \uparrow$	$\mathcal{M}\downarrow$	
Ours	0.801	0.773	0.852	0.076	0.898	0.856	0.954	0.029	0.809	0.711	0.881	0.037	0.842	0.801	0.897	0.047	
Mixup	0.775	0.730	0.834	0.081	0.888	0.839	0.944	0.029	0.783	0.680	0.858	0.042	0.828	0.787	0.887	0.051	

considerable amount of implications about camouflage objects, while the other two methods can not provide comparative depth cues because of their limited training data. Further, we analyse how our model performs with depth estimates from different monocular depth estimation methods, and report the performance in Table 3. "M1" in Table 3 represents directly training the RGB COD branch without using the depth information. LSR [47] is the state-of-theart camouflaged object detection model, "Ours" is our final prediction with the MiDaS depth [58]. "FP" and "MN" are the models with depth maps from FrozenPeople[42]) and Monodepth2[26] respectively. The consistent best performance of "Ours" compared with "FP" and "MN" indicates better depth from MiDaS [58] for our task. We also notice better performance of "FP" and "MN" compared with "M1", which explains the effectiveness of our solution with depth maps from different monocular depth estimation methods. Further, we find better or comparable performance of "FP" and "MN" with "LSR", which again proves the superiority of our solution.

**Depth mixup vs depth selection:** We introduce the depth quality assessment module to assess the depth quality, thus decide which branch (RGB COD or RGB-D COD) to be used during testing. Following [31], we also tried the depth mixup strategy as shown in Algorithm 2. Specifically, we first estimate the depth quality, then we perform depth evolving via self-calibration to obtain the mixuped depth.

#### a) Positive/Negative sample generation

We aim to assess the quality of depth provided with existing monocular depth estimation methods. To do so, we need to select positive samples  $C_p$  and negative samples  $C_n$  representing those that contribute the most and least to camouflaged object detection. To achieve this, we train two camouflaged object detection network with RGB images and RGB-D image pairs respectively, which is defined as  $f_{\theta_1}$  and  $f_{\theta_2}$ . Then we compare the MAE of each sample with each model, and define depth that leads to smaller MAE as positive depth. We formulate this step as below:

$$C_r = MAE(f_{\theta_1}(x_i)) - MAE(f_{\theta_2}(x_i)). \tag{5}$$

We define samples with  $C_r > 0$  as positive samples,  $C_r < 0$  as negative samples.

# Algorithm 2 Depth-Guided Learning

#### Input

Training dataset  $D = \{x_i, d_i, y_i\}_{i=1}^N$ , where the depth map  $d_i$  is pre-computed from existing monocular depth estimation technique.

**Output**: Model parameter  $\theta$  for the RGB COD branch,  $\beta$  for the RGB-D COD branch, and  $\gamma$  for the depth assessment module;

- 1: Generate initial depth maps  $d_i$  for  $x_i$  with existing monocular depth estimation method [58];
- 2: Train a RGB camouflaged object detection network  $f_{\theta_1}$ ;
- 3: Train a joint RGB-D camouflaged object detection and depth estimation network  $f_{\theta_2}$ ;
- 4: Select samples  $C_p$  and  $C_n$  that  $d_i$  contributes the most and least respectively by comparing  $f_{\theta_1}(x)$  and  $f_{\theta_1}(x)$ ;
- 5: Train with  $C_b$  and  $C_s$  as positive samples and negative samples to achieve depth contribution estimation  $f_{\gamma}$ ;
- 6: Obtain the refined depth via self-calibration in Eq.7.
- 7: Train the joint RGB-D camouflaged object detection and depth estimation network  $f_{\theta_2}$  with refined depth as supervision for the depth estimation module.

# b) Depth contribution estimation

The positive depth set  $C_p$  and negative depth set  $C_n$  represent depth that contribute the most and least for camouflaged object detection. We then train a binary classification model  $f_\gamma$  to estimate the contribution of depth from our precomputed. We define the depth contribution as:

$$p_c = f_{\gamma}(x, d) \in [0, 1],$$
 (6)

which represents the contribution of depth maps.

c) Depth evolving via self-calibration

With the depth contribution estimation network  $f_{\gamma}$ , we aim to estimate the contribution of each depth maps  $d_i$ . Following the self-calibration pipeline, one can refine the initial depth as following:

$$d_i^e = p * d_i + (1 - p) * d_a, (7)$$

Table 5. Performance of RGB-D SOD models with our pipeline.

		NJU2	K [33]		SSB [49]					DES	S [6]			NLPF	R [52]		LFSD [40]				SIP [16]			
Method	$S_{\alpha} \uparrow$	$F_{\beta} \uparrow$	$E_{\xi} \uparrow$	$\mathcal{M}\downarrow$	$S_{\alpha} \uparrow$	$F_{\beta} \uparrow$	$E_{\xi} \uparrow$	$\mathcal{M}\downarrow$	$S_{\alpha} \uparrow$	$F_{\beta} \uparrow$	$E_{\xi} \uparrow$	$\mathcal{M}\downarrow$	$S_{\alpha} \uparrow$	$F_{\beta} \uparrow$	$E_{\xi} \uparrow$	$\mathcal{M}\downarrow$	$S_{\alpha} \uparrow$	$F_{\beta} \uparrow$	$E_{\xi} \uparrow$	$\mathcal{M}\downarrow$	$S_{\alpha} \uparrow$	$F_{\beta} \uparrow$	$E_{\xi} \uparrow$	$\mathcal{M}\downarrow$
BBSNet [17]	.921	.902	.938	.035	.908	.883	.928	.041	.933	.910	.949	.021	.930	.896	.950	.023	.864	.843	.883	.072	.879	.868	.906	.055
Raw	.917	.904	.945	.033	.903	.877	.933	.041	.938	.922	.971	.017	.920	.894	.949	.026	.865	.843	.899	.066	.886	.880	.923	.046
Ours_Gen	.917	.909	.943	.036	.902	.881	.934	.039	.940	.926	.973	.016	.918	.889	.949	.025	.831	.819	.867	.084	.880	.873	.914	.050
Ours_Raw	.921	.914	.946	.031	.906	.887	.938	.038	.942	.933	.975	.015	.925	.897	.956	.024	.864	.839	.891	.067	.889	.893	.934	.043

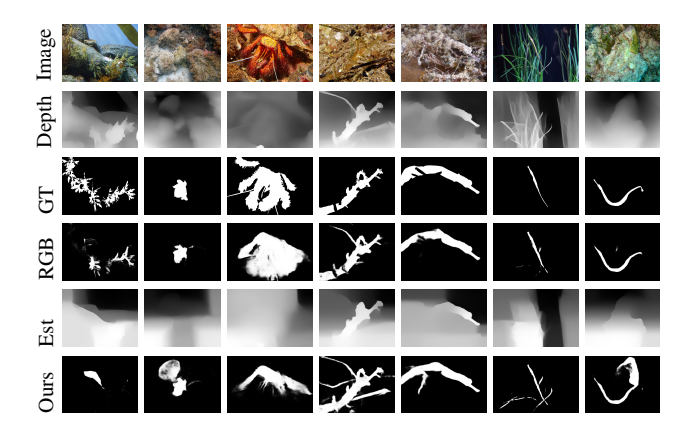


Figure 9. Failure cases analysis.

where  $d_a$  is obtained through the auxiliary depth estimation module. The basic assumption is that if the depth quality is high, we trust it more, otherwise, we update the supervision signal for the depth estimation module with the estimated depth as guidance. We show the performance of this model in Table 4 ("Mixup"). The inferior performance of "Mixup" compared with our final prediction indicates that the hard selection of high quality depth works better in our scenario than the soft combination of depth.

Failure case analysis: Although our proposed depth guided RGB-D COD network performs better than the RGB COD network in general, there still exists samples where our method perform worse than the RGB COD counterpart as shown in Fig. 9, where "Est" is the estimated depth with monocular depth estimation method [58]. The main reasons lie in two parts: 1) the limited representative ability of the depth estimation module; 2) the correctness degree of our assumption for the depth quality assessment module. For the former, we will investigate more effective depth estimation modules as future work. For the latter, we will find other solutions to assess the depth quality for RGB-D camouflaged object detection.

### 4.5. Extension

As a basic RGB-D binary segmentation network, we argue that our solution can be easily extend to other RGB-D binary segmentation task, *e.g.* RGB-D salient object detection (SOD). We then train our model for RGB-D SOD with generated depth and raw depth respectively. Follow-

ing the conventional RGB-D SOD setting [83], we use the combination of 1,485 images from the NJU2K [33] and 700 images from the NLPR [52] as training dataset, and then test on the NJU2K testing set, NLPR testing set, LFSD [40], DES [6], SSB [49] and SIP [16]. For the "raw depth" experiment, we use the original depth maps of the corresponding training and testing dataset. For the "generated depth" experiment, we use generated depth using the monocular depth estimation method, namely Mi-DaS [58] depth in particular. The performance is shown as "Ours\_Gen" (with generated depth) and "Ours\_Raw" (with raw depth) in Table 5, where "Raw" is RGB-D SOD with raw depth using framework in Fig. 4, and "BBSNet" is one SOTA RGB-D SOD model. The competing performance of "Ours\_Gen" and better performance of "Ours\_Raw" compared with "SOTA" and "Raw" illustrates the effectiveness of our model.

# 5. Conclusion

In this paper, we tackle the problem of camouflaged object detection (COD) with the aid of depth. As there exists no dataset with both COD annotations and depth maps, we proposed the first depth-guided COD network, where the depth information is introduced from a monocular depth estimation network. To address the domain gap, we introduced a depth quality assessment module to evaluate the quality of depth based on the COD prediction from both RGB COD branch and RGB-D COD branch. During training, only high-quality depth is used to update the modal interaction module for multi-modal learning. During testing, our depth quality assessment module effectively determines the contribution of depth and selects either the RGB branch or the RGB-D branch. Experimental results on benchmarking dataset prove the superiority of our solution. As an extension, we perform RGB-D salient object detection using our framework with depth generated with the monocular depth estimation methods [58]. The competing performance of our model using generated depth compared with model using raw depth further explains superior performance of our framework. In future, we plan to collect the RGB-D COD dataset and stereo COD dataset to further boost the research in the community.

# References

- Wendy J Adams, Erich W Graf, and Matt Anderson. Disruptive coloration and binocular disparity: breaking camouflage. Proceedings of the Royal Society B, 286(1896):20182045, 2019. 1, 2
- [2] Nagappa U Bhajantri and P Nagabhushan. Camouflage defect identification: a novel approach. In *International Conference on Information Technology*, pages 145–148. IEEE, 2006. 2
- [3] Hao Chen and Youfu Li. Progressively complementarity-aware fusion network for rgb-d salient object detection. In *Proc. IEEE Conf. Comp. Vis. Patt. Recogn.*, pages 3051–3060, 2018.
- [4] Liang-Chieh Chen, George Papandreou, Iasonas Kokkinos, Kevin Murphy, and Alan L Yuille. Deeplab: Semantic image segmentation with deep convolutional nets, atrous convolution, and fully connected crfs. *IEEE Trans. Pattern Anal. Mach. Intell.*, 40(4):834–848, 2017. 1, 4
- [5] Shuhan Chen, Xiuli Tan, Ben Wang, Huchuan Lu, Xuelong Hu, and Yun Fu. Reverse attention-based residual network for salient object detection. *IEEE Trans. Image Proc.*, 29:3763–3776, 2020. 7
- [6] Yupeng Cheng, Huazhu Fu, Xingxing Wei, Jiangjian Xiao, and Xiaochun Cao. Depth enhanced saliency detection method. In *Proceedings of international conference on internet multimedia computing and service*, pages 23–27, 2014.
- [7] Anthony C Copeland and Mohan M Trivedi. Models and metrics for signature strength evaluation of camouflaged targets. In *Algorithms for synthetic aperture radar imagery IV*, volume 3070, pages 194–199, 1997. 1, 2
- [8] Shuanglu Dai and Hong Man. A convolutional riemannian texture model with differential entropic active contours for unsupervised pest detection. In *IEEE International Conference on Acoustics, Speech and Signal Processing*, pages 1028–1032, 2017. 1
- [9] Zhuo Deng, Sinisa Todorovic, and Longin Jan Latecki. Semantic segmentation of rgbd images with mutex constraints. In *Proc. IEEE Conf. Comp. Vis. Patt. Recogn.*, pages 1733–1741, 2015.
- [10] Thomas G. Dietterich. Ensemble methods in machine learning. In *Proceedings of the First International Workshop on Multiple Classifier Systems*, pages 1–15, 2000. 3
- [11] Bo Dong, Mingchen Zhuge, Yongxiong Wang, Hongbo Bi, and Geng Chen. Towards accurate camouflaged object detection with mixture convolution and interactive fusion. *arXiv* preprint arXiv:2101.05687, 2021. 1, 2
- [12] Deng-Ping Fan, Ming-Ming Cheng, Yun Liu, Tao Li, and Ali Borji. Structure-measure: A new way to evaluate foreground maps. In *Proc. IEEE Int. Conf. Comp. Vis.*, pages 4548– 4557, 2017. 6
- [13] Deng-Ping Fan, Cheng Gong, Yang Cao, Bo Ren, Ming-Ming Cheng, and Ali Borji. Enhanced-alignment measure for binary foreground map evaluation. In *Proc. IEEE Int. Joint Conf. Artificial Intell.*, pages 698–704, 2018. 6
- [14] Deng-Ping Fan, Ge-Peng Ji, Guolei Sun, Ming-Ming Cheng, Jianbing Shen, and Ling Shao. Camouflaged object detec-

- tion. In *Proc. IEEE Conf. Comp. Vis. Patt. Recogn.*, pages 2777–2787, 2020. 1, 2, 3, 6, 7, 8, 9
- [15] Deng-Ping Fan, Ge-Peng Ji, Tao Zhou, Geng Chen, Huazhu Fu, Jianbing Shen, and Ling Shao. Pranet: Parallel reverse attention network for polyp segmentation. In *International Conference on Medical Image Computing and Computer-Assisted Intervention*, pages 263–273, 2020. 1
- [16] Deng-Ping Fan, Zheng Lin, Zhao Zhang, Menglong Zhu, and Ming-Ming Cheng. Rethinking RGB-D Salient Object Detection: Models, Datasets, and Large-Scale Benchmarks. *IEEE Transactions on neural networks and learning systems*, 2020, 10
- [17] Deng-Ping Fan, Yingjie Zhai, Ali Borji, Jufeng Yang, and Ling Shao. Bbs-net: Rgb-d salient object detection with a bifurcated backbone strategy network. In *Proc. Eur. Conf. Comp. Vis.*, pages 275–292, 2020. 2, 7, 10
- [18] Zheng Fang, Xiongwei Zhang, Xiaotong Deng, Tieyong Cao, and Changyan Zheng. Camouflage people detection via strong semantic dilation network. In *Proceedings of the ACM Turing Celebration Conference-China*, pages 1–7, 2019.
- [19] Clement Farabet, Camille Couprie, Laurent Najman, and Yann LeCun. Learning hierarchical features for scene labeling. *IEEE Trans. Pattern Anal. Mach. Intell.*, 35(8):1915– 1929, 2012. 2
- [20] David Feng, Nick Barnes, Shaodi You, and Chris McCarthy. Local background enclosure for rgb-d salient object detection. In *Proc. IEEE Conf. Comp. Vis. Patt. Recogn.*, pages 2343–2350, 2016.
- [21] Mengyang Feng, Huchuan Lu, and Yizhou Yu. Residual learning for salient object detection. *IEEE Trans. Image Proc.*, 29:4696–4708, 2020. 7
- [22] Xue Feng, Cui Guoying, Hong Richang, and Gu Jing. Camouflage texture evaluation using a saliency map. *Multimedia Systems*, 21(2):169–175, 2015. 2
- [23] Keren Fu, Deng-Ping Fan, Ge-Peng Ji, and Qijun Zhao. Jl-dcf: Joint learning and densely-cooperative fusion framework for rgb-d salient object detection. In *Proc. IEEE Conf. Comp. Vis. Patt. Recogn.*, pages 3052–3062, 2020. 7
- [24] Yarin Gal and Zoubin Ghahramani. Dropout as a Bayesian approximation: Representing model uncertainty in deep learning. In *Proc. Int. Conf. Mach. Learn.*, pages 1050–1059, 2016.
- [25] Shang-Hua Gao, Yong-Qiang Tan, Ming-Ming Cheng, Chengze Lu, Yunpeng Chen, and Shuicheng Yan. Highly efficient salient object detection with 100k parameters. In Proc. Eur. Conf. Comp. Vis., pages 702–721, 2020. 7
- [26] Clément Godard, Oisin Mac Aodha, Michael Firman, and Gabriel J. Brostow. Digging into self-supervised monocular depth prediction. In *Proc. IEEE Int. Conf. Comp. Vis.*, pages 3828–3838, 2019. 3, 4, 8, 9
- [27] Saurabh Gupta, Pablo Arbelaez, and Jitendra Malik. Perceptual organization and recognition of indoor scenes from rgb-d images. In *Proc. IEEE Conf. Comp. Vis. Patt. Recogn.*, pages 564–571, 2013. 2
- [28] Joanna R Hall, Olivia Matthews, Timothy N Volonakis, Eric Liggins, Karl P Lymer, Roland Baddeley, Innes C Cuthill, and Nicholas E Scott-Samuel. A platform for initial testing

- of multiple camouflage patterns. *Defence Technology*, 2020.
- [29] Kaiming He, Georgia Gkioxari, Piotr Dollár, and Ross Girshick. Mask r-cnn. In *Proc. IEEE Int. Conf. Comp. Vis.*, pages 2961–2969, 2017.
- [30] Kaiming He, Xiangyu Zhang, Shaoqing Ren, and Jian Sun. Deep residual learning for image recognition. In *Proc. IEEE Conf. Comp. Vis. Patt. Recogn.*, pages 770–778, 2016. 4
- [31] Zhang Hongyi, Cisse Moustapha, Dauphin Yann N., and Lopez-Paz David. mixup: Beyond empirical risk minimization. In *Proc. Int. Conf. Learning Representations*, 2018. 9
- [32] Xinxin Hu, Kailun Yang, Lei Fei, and Kaiwei Wang. Acnet: Attention based network to exploit complementary features for rgbd semantic segmentation. In *Proc. IEEE Int. Conf. Image Process.*, pages 1440–1444, 2019.
- [33] Ran Ju, Yang Liu, Tongwei Ren, Ling Ge, and Gangshan Wu. Depth-aware salient object detection using anisotropic center-surround difference. Signal Processing: Image Communication, 38:115–126, 2015. 10
- [34] Emma J Kelman, Daniel Osorio, and Roland J Baddeley. A review of cuttlefish camouflage and object recognition and evidence for depth perception. *Journal of Experimental Biology*, 211(11):1757–1763, 2008. 1, 2
- [35] Alex Kendall and Yarin Gal. What uncertainties do we need in bayesian deep learning for computer vision? In *Proc. Adv. Neural Inf. Process. Syst.*, pages 5580–5590, 2017.
- [36] Lingkai Kong, Jimeng Sun, and Chao Zhang. Sde-net: Equipping deep neural networks with uncertainty estimates. *Proc. Int. Conf. Mach. Learn.*, pages 5405–5415, 2020. 3
- [37] Balaji Lakshminarayanan, Alexander Pritzel, and Charles Blundell. Simple and scalable predictive uncertainty estimation using deep ensembles. In *Proc. Adv. Neural Inf. Process. Syst.*, pages 6402–6413, 2017. 3
- [38] Trung-Nghia Le, Tam V Nguyen, Zhongliang Nie, Minh-Triet Tran, and Akihiro Sugimoto. Anabranch network for camouflaged object segmentation. *Comp. Vis. Image Under*standing, 184:45–56, 2019. 1, 2, 3, 6, 7, 8, 9
- [39] Simcha Lev-Yadun, Amots Dafni, Moshe A Flaishman, Moshe Inbar, Ido Izhaki, Gadi Katzir, and Gidi Ne'eman. Plant coloration undermines herbivorous insect camouflage. *BioEssays*, 26(10):1126–1130, 2004.
- [40] Nianyi Li, Jinwei Ye, Yu Ji, Haibin Ling, and Jingyi Yu. Saliency detection on light field. In *Proc. IEEE Conf. Comp. Vis. Patt. Recogn.*, pages 2806–2813, 2014. 10
- [41] Shuai. Li, Dinei. Florencio, Wanqing Li, Yaqin Zhao, and Chris Cook. A fusion framework for camouflaged moving foreground detection in the wavelet domain. *IEEE Trans. Image Proc.*, 27(8):3918–3930, 2018.
- [42] Zhengqi Li, Tali Dekel, Forrester Cole, Richard Tucker, Noah Snavely, Ce Liu, and William T Freeman. Learning the depths of moving people by watching frozen people. In Proc. IEEE Conf. Comp. Vis. Patt. Recogn., pages 4521– 4530, 2019. 3, 4, 9
- [43] Di Lin, Guangyong Chen, Daniel Cohen-Or, Pheng-Ann Heng, and Hui Huang. Cascaded feature network for semantic segmentation of rgb-d images. In *Proc. IEEE Int. Conf. Comp. Vis.*, pages 1311–1319, 2017. 2

- [44] Jiang-Jiang Liu, Qibin Hou, Ming-Ming Cheng, Jiashi Feng, and Jianmin Jiang. A simple pooling-based design for real-time salient object detection. In *Proc. IEEE Conf. Comp. Vis. Patt. Recogn.*, pages 3917–3926, 2019.
- [45] Nian Liu, Ni Zhang, and Junwei Han. Learning selective self-mutual attention for rgb-d saliency detection. In *Proc. IEEE Conf. Comp. Vis. Patt. Recogn.*, pages 13756–13765, 2020. 2
- [46] Jonathan Long, Evan Shelhamer, and Trevor Darrell. Fully convolutional networks for semantic segmentation. In *Proc. IEEE Conf. Comp. Vis. Patt. Recogn.*, pages 3431–3440, 2015. 2
- [47] Yunqiu Lv, Jing Zhang, Yuchao Dai, Aixuan Li, Bowen Liu, Nick Barnes, and Deng-Ping Fan. Simultaneously localize, segment and rank the camouflaged objects. In *Proc. IEEE Conf. Comp. Vis. Patt. Recogn.*, 2021. 3, 6, 7, 8, 9
- [48] Melia G Nafus, Jennifer M Germano, Jeanette A Perry, Brian D Todd, Allyson Walsh, and Ronald R Swaisgood. Hiding in plain sight: a study on camouflage and habitat selection in a slow-moving desert herbivore. *Behavioral Ecol*ogy, 26(5):1389–1394, 2015. 1
- [49] Yuzhen Niu, Yujie Geng, Xueqing Li, and Feng Liu. Leveraging stereopsis for saliency analysis. In *Proc. IEEE Conf. Comp. Vis. Patt. Recogn.*, pages 454–461, 2012. 10
- [50] Seong-Jin Park, Ki-Sang Hong, and Seungyong Lee. Rdfnet: Rgb-d multi-level residual feature fusion for indoor semantic segmentation. In *Proc. IEEE Int. Conf. Comp. Vis.*, pages 4980–4989, 2017. 2
- [51] Olivier Penacchio, P George Lovell, Innes C Cuthill, Graeme D Ruxton, and Julie M Harris. Three-dimensional camouflage: exploiting photons to conceal form. *The American Naturalist*, 186(4):553–563, 2015. 2
- [52] Houwen Peng, Bing Li, Weihua Xiong, Weiming Hu, and Rongrong Ji. RGBD salient object detection: A benchmark and algorithms. In *Proc. Eur. Conf. Comp. Vis.*, pages 92– 109, 2014. 2, 10
- [53] Yongri Piao, Wei Ji, Jingjing Li, Miao Zhang, and Huchuan Lu. Depth-induced multi-scale recurrent attention network for saliency detection. In *Proc. IEEE Int. Conf. Comp. Vis.*, pages 7254–7263, 2019. 2
- [54] Thomas W Pike. Quantifying camouflage and conspicuousness using visual salience. *Methods in Ecology and Evolution*, 9(8):1883–1895, 2018. 2
- [55] Natasha Price, Samuel Green, Jolyon Troscianko, Tom Tregenza, and Martin Stevens. Background matching and disruptive coloration as habitat-specific strategies for camouflage. Scientific reports, 9(1):1–10, 2019. 1
- [56] Chen Qian, Hongsheng Li, and Gang Zeng. Bi-directional cross-modality feature propagation with separation-andaggregation gate for rgb-d semantic segmentation. In *Proc. Eur. Conf. Comp. Vis.*, pages 561—577, 2020. 2
- [57] Xuebin Qin, Zichen Zhang, Chenyang Huang, Chao Gao, Masood Dehghan, and Martin Jagersand. Basnet: Boundaryaware salient object detection. In *Proc. IEEE Conf. Comp. Vis. Patt. Recogn.*, pages 7479–7489, June 2019. 7
- [58] René Ranftl, Katrin Lasinger, David Hafner, Konrad Schindler, and Vladlen Koltun. Towards robust monocular

- depth estimation: Mixing datasets for zero-shot cross-dataset transfer. *IEEE Trans. Pattern Anal. Mach. Intell.*, 2020. 2, 3, 4, 6, 7, 8, 9, 10
- [59] Joseph Redmon, Santosh Divvala, Ross Girshick, and Ali Farhadi. You only look once: Unified, real-time object detection. In *Proc. IEEE Conf. Comp. Vis. Patt. Recogn.*, pages 779–788, 2016. 1
- [60] Jianqiang Ren, Xiaojin Gong, Lu Yu, Wenhui Zhou, and Michael Ying Yang. Exploiting global priors for rgb-d saliency detection. In *Proc. IEEE Conf. Comp. Vis. Patt. Recogn. Workshops*, pages 25–32, 2015. 2
- [61] Xiaofeng Ren, Liefeng Bo, and Dieter Fox. Rgb-(d) scene labeling: Features and algorithms. In Proc. IEEE Conf. Comp. Vis. Patt. Recogn., pages 2759–2766, 2012.
- [62] Olaf Ronneberger, Philipp Fischer, and Thomas Brox. Unet: Convolutional networks for biomedical image segmentation. In *International Conference on Medical image computing and computer-assisted intervention*, pages 234–241, 2015.
- [63] Yichen Shen, Zhilu Zhang, Mert R Sabuncu, and Lin Sun. Real-time uncertainty estimation in computer vision via uncertainty-aware distribution distillation. In *Proc. IEEE Winter Conf. on App. of Comp. Vis.*, pages 707–716, 2021.
- [64] Nathan Silberman and Rob Fergus. Indoor scene segmentation using a structured light sensor. In *Proc. IEEE Int. Conf. Comp. Vis. Workshops*, pages 601–608, 2011. 2
- [65] Przemysław Skurowski, Hassan Abdulameer, Jakub Baszczyk, Tomasz Depta, Adam Kornacki, and Przemysław Kozie. Animal camouflage analysis: Chameleon database. In *Unpublished Manuscript*, 2018. 7, 8, 9
- [66] Ariel Tankus and Yehezkel Yeshurun. Convexity-based visual camouflage breaking. Comp. Vis. Image Understanding, 82(3):208–237, 2001. 2
- [67] Gerald Handerson Thayer. Concealing-coloration in the animal kingdom: an exposition of the laws of disguise through color and pattern. Macmillan Company, 1918. 1
- [68] Abhinav Valada, Rohit Mohan, and Wolfram Burgard. Self-supervised model adaptation for multimodal semantic segmentation. *Int. J. Comp. Vis.*, pages 1–47, 2019.
- [69] Anzhi Wang and Minghui Wang. Rgb-d salient object detection via minimum barrier distance transform and saliency fusion. *IEEE Signal Process. Lett.*, 24(5):663–667, 2017.
- [70] Yang Wang, Yi Yang, Zhenheng Yang, Liang Zhao, Peng Wang, and Wei Xu. Occlusion aware unsupervised learning of optical flow. In *Proc. IEEE Conf. Comp. Vis. Patt. Recogn.*, pages 4884–4893, 2018. 5, 6, 8
- [71] Jun Wei, Shuhui Wang, and Qingming Huang. F<sup>3</sup>net: Fusion, feedback and focus for salient object detection. In *Proc. AAAI Conf. Artificial Intelligence*, pages 12321–12328, 2020. 7
- [72] Evan C Wilson, Amy A Shipley, Benjamin Zuckerberg, M Zachariah Peery, and Jonathan N Pauli. An experimental translocation identifies habitat features that buffer camouflage mismatch in snowshoe hares. *Conservation Letters*, 12(2):12614, 2019.

- [73] Zhe Wu, Li Su, and Qingming Huang. Cascaded partial decoder for fast and accurate salient object detection. In Proc. IEEE Conf. Comp. Vis. Patt. Recogn., pages 3907– 3916, 2019. 7
- [74] Zhe Wu, Li Su, and Qingming Huang. Stacked cross refinement network for edge-aware salient object detection. In *Proc. IEEE Int. Conf. Comp. Vis.*, pages 7264–7273, 2019. 7
- [75] Feng Xue, Chengxi Yong, Shan Xu, Hao Dong, Yuetong Luo, and Wei Jia. Camouflage performance analysis and evaluation framework based on features fusion. *Multimedia Tools and Applications*, 75(7):4065–4082, 2016.
- [76] Jinnan Yan, Trung-Nghia Le, Khanh-Duy Nguyen, Minh-Triet Tran, Thanh-Toan Do, and Tam V Nguyen. Mirrornet: Bio-inspired adversarial attack for camouflaged object segmentation. arXiv preprint arXiv:2007.12881, 2020. 1, 2, 3, 6
- [77] Jing Zhang, Deng-Ping Fan, Yuchao Dai, Saeed Anwar, Fatemeh Sadat Saleh, Tong Zhang, and Nick Barnes. Uc-net: Uncertainty inspired rgb-d saliency detection via conditional variational autoencoders. In *Proc. IEEE Conf. Comp. Vis. Patt. Recogn.*, pages 8582–8591, 2020. 2, 7
- [78] Miao Zhang, Weisong Ren, Yongri Piao, Zhengkun Rong, and Huchuan Lu. Select, supplement and focus for rgb-d saliency detection. In *Proc. IEEE Conf. Comp. Vis. Patt. Recogn.*, pages 3472–3481, 2020. 7
- [79] Yulun Zhang, Kunpeng Li, Kai Li, Lichen Wang, Bineng Zhong, and Yun Fu. Image super-resolution using very deep residual channel attention networks. In *Proc. Eur. Conf. Comp. Vis.*, pages 286–301, 2018. 4
- [80] Jia-Xing Zhao, Jiang-Jiang Liu, Deng-Ping Fan, Yang Cao, Jufeng Yang, and Ming-Ming Cheng. Egnet: Edge guidance network for salient object detection. In *Proc. IEEE Int. Conf. Comp. Vis.*, pages 8779–8788, 2019.
- [81] Yunfei Zheng, Xiongwei Zhang, Feng Wang, Tieyong Cao, Meng Sun, and Xiaobing Wang. Detection of people with camouflage pattern via dense deconvolution network. *IEEE Signal Process. Lett.*, 26(1):29–33, 2018.
- [82] Huajun Zhou, Xiaohua Xie, Jian-Huang Lai, Zixuan Chen, and Lingxiao Yang. Interactive two-stream decoder for accurate and fast saliency detection. In *Proc. IEEE Conf. Comp. Vis. Patt. Recogn.*, pages 9141–9150, 2020. 7
- [83] Tao Zhou, Deng-Ping Fan, Ming-Ming Cheng, Jianbing Shen, and Ling Shao. RGB-D salient object detection: A survey. Computational Visual Media, pages 37–69, 2021. 10